HHS Public Access

Author manuscript

Semin Nephrol. Author manuscript; available in PMC 2021 January 26.

Published in final edited form as:

Semin Nephrol. 2019 July ; 39(4): 316–327. doi:10.1016/j.semnephrol.2019.04.002.

Acid-Base Basics

Michael F. Romero, PhD, **Adam J. Rossano, MD, PhD**

Physiology and Biomedical Engineering, Nephrology and Hypertension, Mayo Clinic College of Medicine and Science, Rochester, MN

Summary:

Although students initially learn of ionic buffering in basic chemistry, buffering and acid-base transport in biology often is relegated to specialized classes, discussions, or situations. That said, for physiology, nephrology, pulmonology, and anesthesiology, these basic principles often are critically important for mechanistic understanding, medical treatments, and assessing therapy effectiveness. This short introductory perspective focuses on basic chemistry and transport of buffers and acid-base equivalents, provides an outline of basic science acid-base concepts, tools used to monitor intracellular pH, model cellular responses to pH buffer changes, and the more recent development and use of genetically encoded pH-indicators. Examples of newer genetically encoded pH-indicators (pHerry and pHire) are provided, and their use for in vitro, ex vivo, and in vivo experiments are described. The continued use and development of these basic tools provide increasing opportunities for both basic and potentially clinical investigations.

Keywords

Intracellular pH; pH buffering; genetically encoded pH indicator; GEpHI; ammonium pulse; CO_2/HCO_3^- buffering

The hydrogen ion (H^+) (ie, a proton) is the smallest ion, its control in biological systems is critical for life. Because biologic [H^+] vary between 10 nmol/L and 10 mmol/L, pH (ie, -log[a_{H+}], where a_{H+} is H^+ activity) is used for easier reference. Bacteria live and thrive in part because of their ability to maintain a H^+ gradient across their cell membrane. This is accomplished by using H^+ pumps (adenosine triphosphatases) to move H^+ from the intracellular compartment to the outside world, generating the proton motive force (PMF), which has its theoretical framework in Mitchell's[1] chemiosmotic theory. Bacterial uptake of nutrients frequently is coupled to the proton motive force (PMF) via H^+-coupled transporters and voltage-sensitive membrane transporters and channels. Mitchell's[1] chemiosmotic theory, developed to describe membrane permeability to H^+, is generalized to the Gibbs free energy relationship, also known as the electrochemical potential:

Address reprint requests to Michael F. Romero, PhD, Physiology and Biomedical Engineering, Mayo Clinic College of Medicine and Science, 200 First St SW, Rochester, MN 55906. romero.michael@mayo.edu.

Current affiliation of A.J.R.: Department of Psychiatry, The Johns Hopkins School of Medicine, Baltimore, MD.

Conflict of interest statement: M.F.R. is employed by the Mayo Clinic Foundation and has received federal funding to support this area of research.

$$\Delta\mu_{ion} = RT \cdot \ln\{[ion]_{inside}/[ion]_{outside}\} + z_{ion}F\Delta\Psi \quad \text{(equation 1)}$$

F or equation 1, R is the gas constant, T is temperature (Kelvin), ln is the natural log, z is the net particle charge, F is the Faraday constant, and $\Delta\Psi = \Psi(\text{inside}) - \Psi(\text{outside})$ (ie, membrane potential [V_m]). This same electrochemical potential (ie, PMF) allows mitochondria and chloroplasts to convert chemical and voltage gradients to usable cellular energy in the form of adenosine triphosphate. For the specific case of no free energy (ie, $\Delta\mu_{ion} \equiv 0$), this relationship may be rearranged to the Nernst potential:

$$V_{ion} = -\{RT/z_{ion}F\} \cdot \ln\{[ion]_{inside}/[ion]_{outside}\} \quad \text{(equation 2)}$$

WHY MEASURE PH OR INTRACELLULAR pH?

Although quantifying pH in cells, tissues, and organisms might appear as merely a cerebral exercise, there are explicit metabolic and physiologic reasons for this attention. Regulation of intracellular and extracellular pH (acid-base transport) maintains a particular H^+ gradient across cell membranes. Normal cell function is a balance between inward and outward movements of these ions, often varying in response to intracellular pH (pH_i). This is especially true in the central nervous system, digestive tract, heart, respiratory tract, and urinary system.

Many cellular events are pH-sensitive,[2] and some particularly so. Metabolic enzymes, such as the rate-limiting enzyme in glycolysis and phosphofructokinase,[3] and a critical ribosomal protein, S6,[4] move from being fully active to fully inactive with a pH drift of approximately only 0.1. This of course means that if pH_i is not controlled, both cellular energy metabolism and new protein synthesis will stop. A sufficiently alkaline pH_i is required for proliferation in response to several growth factors.[5–7] With so many key processes being pH_i-sensitive, organisms and cells have evolved acid-base transporters, located in the plasma membrane, to regulate pH_i. Not surprisingly, acid-base transporters are controlled by hormones, growth factors, cell volume, intracellular signaling molecules, and phosphorylation.[8–24] In most cells, the most robust and effective of these acid-base transporters carry HCO_3^-. A notable exception are cardiac myocytes for which non-HCO_3^-. transporters control the majority of cellular acid-base flux.[25–27]

ACID-BASE TRANSPORTERS

When thinking of pH and acid-base transporters, most scientists focus on H^+ transport (eg, Na^+-H^+ exchangers; NHE, solute leak carrier 9 [SLC9] gene family). Certainly, these H^+ transporters are very important. However, for most cells, HCO_3^- transporters carry more acid-base equivalents and are more active in a CO_2/HCO_3^- environment. Molecular information had been limited to the Cl^--HCO_3^- exchanger (AE1-AE3), despite rich physiological documentation of HCO_3^- transporters. Since cloning the salamander Ambystoma's electrogenic Na^+/HCO_3^- cotransporter (NBCe1/Slc4a4),[28] modern molecular biology tools have begun an explosive revisiting of HCO_3^- transporter identification, localization, and physiology, and many novel SLC4-HCO_3^- transporters[29,30] and SLC26-

HCO_3^- transporters[31–38] have now been functionally and genomically identified (for more recent reviews, see SLC4 by Romero et al[39] and SLC26 by Alper and Sharma[31]).

In addition to the most common acid (H^+) and base (OH^- and HCO_3^-), there are several other ions and solutes that may accept H^+ (base) or release H^+ (acid) (Table 1). These compounds typically are considered buffers, that is, compounds that can either accept a H^+ or give up a H^+ to maintain pH. These solutes also are considered weak acids or weak bases. Biological H^+ acceptors bases include NH_3, HPO_4^-, lactate$^-$, pyruvate$^-$, and deprotonated organic acids (eg, nicotinate$^-$, butyrate$^-$, propionate$^-$). From the cellular transport side, these substrates fall within several SLC-families (recent reviews and details of SLC families are available at http://slc.bioparadigms.org/) (Table 1): monocarboxylates, SLC5A8 and SLC5A12 (Na^+ coupled), SLC16; dicarboxylates and sulfate, SLC13; phosphates, SLC20 and SLC34; and NH_3/NH_4^+, SLC34. In general these compounds follow the reaction:

$B^- + H^+ \leftrightarrow BH$, where the total buffer concentration ([BH]) equals $[B^-] + [H^+]$. The association/dissociation constant (K) is given by a general equation:

$$K = \{\text{products}\}/\{\text{reactants}\} = \{p\}/\{r\} = \{[BH]\}/\{[B^-]\cdot[H^+]\} \quad \text{(equation 3)}$$

Similarly, this buffer's contribution to pH of a solution or cellular compartment is as follows:

$$pH = pK_{buffer} + \log\{[BH]\}/\{[B^-]\cdot[H^+]\} \quad \text{(equation 4)}$$

For CO_2/HCO_3^-, this equation becomes the Henderson-Haselbach equation:

$$pH = pK_{CO2} + \log\{[HCO_3^-]/[CO_2]\} = 6.1 + \log\{[HCO_3^-]/(s\cdot pCO_2)\} \quad \text{(equation 5)}$$

where $pK_{CO2} = 6.1$ and $s = CO_2$ solubility.

Because pH buffers have different pKs (Table 2), rather than having a single small pH range of buffering, a system of buffers broadens the buffering pH range.[40] This means that total solution or compartment buffering (B_{total}) is as follows:

$$B_{total} = \Sigma(B_1 + B_2 + B_3 + \ldots B_{(n-1)} + B_n) \quad \text{(equation 6)}$$

This relationship of chemical H^+ buffering also is known as the *isohydric principle*. For calculating the pH of a compartment, this transforms to:

$$pH = \Sigma(pK_{B1} + pK_{B2} + pK_{B3} + \ldots . pK_{Bn}) + \log\{\Sigma(p_1 + p_2 + p_3 + \ldots p_n)\}/\{\Sigma(r_1 + r_2 + r_3 + \ldots r_n)\} \quad \text{(equation 7)}$$

In other words, the pH and the solution buffering is determined by the collective contribution of all the solution buffers. Practically, the major buffers in a compartment are used to calculate pH. More frequently, the pH and knowing the specific buffers are used to calculate the ionized or total buffer. Importantly, knowing the buffers in a particular compartment and their respective pKas allows one to determine if pH is effectively controlled or if there is disequilibrium in the system.

pH MEASUREMENT

Because pH regulates critical cellular and systemic processes, being able to accurately and precisely measure pH allows a researcher or clinician to determine what components are at work in a given system (ie, subcellular, cellular, blood, interstitial, or systemic). Early measurements of pH relied on distribution of a membrane-permeant molecule, such as NH_3, CO_2, 5,5-dimethyloxazolidine-2,4-dione (DMO), or amines, which as either weak acids or weak bases may accept or lose a H^+ (for review, see Roos and Boron[41]). DeVris[42] first illustrated this permeant-weak base device by exposing beet slices to NH_3. However, these distributions of permeant molecules are difficult to calibrate to actual pH values.

Perturbing the extracellular environment to elicit a pH_i change is a very useful experimental technique. The most obvious way to change pH_i would be to transport a buffer (eg, NH_4^+, HCO_3^-) across the plasma membrane of a cell (Fig. 1 illustrates NH_4^+ effects, Fig. 2 illustrates HCO_3^- effects). Transport of each buffer can be accomplished by one of the previously mentioned SLC transporters (HCO_3^- by SLC4[39] and SLC26[31], and NH_3 and NH_4^+ by SLC[42,43]). In the mid-1970s, Boron and De Weer[44] described pH_i changes in squid giant axon resulting from the presence of NH_3 or CO_2 in their extracellular solutions.

NH_3 AND $NH_4^{\pm}$ TRANSPORT

In the case of NH_3, dissolving NH_4Cl in solution releases NH_4^+ into solution that is in a steady-state with NH_3 and H^+ (Fig. 1). Despite a pKa of 9.2 (Table 2), a 10 mmol/L NH_4Cl solution contains approximately 10 μmol/L NH_3. Figure 1 shows a model response of a cell to the addition of NH_4Cl. This addition elicits a two-phase, pH_i response (Fig. 1): phase one is a fast NH_3 permeation of the cell membrane (likely a channel) causing a fast pH_i increase (Fig. 1A–a), and phase two is a slower transporter-mediated acidification (decrease in pH_i; Fig. 1A–b). The initial NH_3 channel[45–50] has not been explicitly determined for every cell type. The concept was developed with the finding by Kikeri et al[45] that the apical membranes of mammalian thick ascending limb were not able to pass NH_3. Later, Boron's and Geibel's laboratories showed that gastric glands and colonic crypts also have virtually no apical NH_3 permeability.[46,51] Later, the molecular path for NH_3 was shown in several proteins: AmtB[47] and certain aquaporins[48] and RhCG proteins.[48–50] The most striking example from Khademi et al[47] shown using a 1.35Å resolution AmtB crystal structure, is that NH_4^+ is too big for the pore and that only NH_3 can fit. It should be noted that *Xenopus* oocytes, a commonly used protein expression system, lack proteins that act as NH_3 channels.[48] Consequently, in these cells, NH_4Cl addition only results in an acidification (phase two).

The second phase is NH_4^+ transport (Fig. 1A–b). When NH_4^+ moves into a cell at this increased pH_i (ie, closer to the pKa), NH_4^+ will dissociate to NH_3 and H^+ (acidification or decreasing pH_i). In the continued presence of NH_4Cl, this acidification will continue until a new steady-state is reached. Phase one and phase two together often are referred to as an ammonium prepulse.[44]

Removal of NH_4Cl

Once a cell has been loaded with this additional NH_3/NH_4^+ buffer, acute removal of the NH_4Cl-containing solution results in a reversal of these two phases, albeit with different transport implications. Pha'se one is again the rapid transit of NH_3 (Fig. 1A–c), which results in an increase of intracellular H^+ (rapid acidification) as NH_4^+ dissociates. Phase two (compare Fig. 1A–d with Fig. 1A–d') with NH_4Cl removal is often the most useful from the ion transport perspective. Once the cell has moved to an extreme acidification, the recovery (alkalization) is the composite of all of the acid-extruding systems (H^+ efflux or HCO_3^- influx, see later). In this second phase, replacement of ions, removal of coupled substrates, or addition of inhibitors are used to fingerprint physiologic mechanism of acid extrusion (Fig. 1A–d'). For example, if Na^+ is replaced by an impermeant cation, the Na^+/H^+ exchanger shown likely would stop because more H^+ could not be brought into the cell easily. Similarly, addition of amiloride or ethyl-isopropyl amiloride would inhibit Na^+/H^+ exchangers such that the cell would not recover from the acidification.

CO_2/HCO_3^- ADDITION TO MAMMALIAN CELLS

Another experimental maneuver, which shows the magnitudes of acid or base fluxes more appropriately, is the abrupt addition of CO_2/HCO_3^- to solution bathing a cell whose pH_i is being monitored. This, of course, is more physiologic because CO_2 is one of the products of cellular respiration. Similar to the NH_4^+ prepulse, addition of a CO_2/HCO_3^- equilibrated solution elicits an initial rapid pH_i change. However, as CO_2 enters the cell, it hydrates to form H_2CO_3, which then quickly dissociates to HCO_{3-} and H^+ (acidification, acid loading, or base extrusion) (Fig. 2A–a and B–a). In the presence of a carbonic anhydrase, CO_2 and H_2O are bound and converted enzymatically to HCO_3^- and H^+, which typically would increase the rate, but not amount, of acidification.

In the presence of CO_2/HCO_3^-, transport systems that require HCO_3^- become active (Fig. 2A–b and B–b) (eg, a Na^+ bicarbonate cotransport: NBCe1, SLC4A4). In this case, HCO_3^- directly enters the cell as HCO_3^-, causing an alkalization (increased pH_i; base-loading = acid extrusion). If we assume that this is a 5% CO_2 solution at room temperature (25 mmol/L HCO_3^-) (Fig. 2B), $[HCO_3^-]$ at the a-b (pH 7.0; ~10 mmol/L) and b-c (pH 7.4; ~26 mmol/L) junctions can be calculated by rearrangement of the Henderson-Haselbach equation. This means that the HCO_3^- loading (intracellular buffering) in Figure 2B (ie, $\Delta[HCO_3^-]$) is 16 mmol/L. If there are no HCO_3^- transporters to allow the HCO_3^- ion to enter the cell, then the chemistry follows the scheme illustrated in Figure 2A–a' and A–b' (Fig. 2B, red lines). The initial decrease in pH_i is much larger (0.4 pH units), and b' has a slope of zero. The steady-state pH_i of 6.8 means that intracellular $[HCO_3^-]$ is 6.5 mmol/L rather than 10 mmol/L. The HCO_3^- loading in Figure 2B–b versus Figure 2B–b' shows that

this active base-loading system increases [HCO_3^-] at b-c versus b'-c' by more than 16 mmol/L.

When the CO_2/HCO_3^- is removed from the solution, any HCO_3^- formed by CO_2 hydration or transported into the cell will be reunited with H^+ to form H_2O and CO_2. The CO_2 then quickly exits the cell (Fig. 2A–c, A–c' and B–c and B–c'). Once again, the wave forms differ owing to the presence of one or more HCO_3^- transporters, which may not completely reverse on the same short time scale.

Cellular and subcellular pH also has been measured using a variety of pH buffers that take advantage of color changes, absorbance, or fluorescence. Classic pH measurement techniques have been reviewed previously.[41] The gold standard for pH measurement (solution pH or pHi) is a pH electrode because this measurement technique shows high sensitivity over greater than 6 decades of [H^+].

pH ELECTRODES

Electrodes to measure pH in biological solutions fall into three broad classes: blackened Pt wire, pH-sensitive glass, or a resin-encapsulated protonophore in a micropipette. The basic principle is that for every 10-fold change in [H^+], pH unit, the voltage measured by the electrode changes approximately 60 mV. This voltage change per pH unit is the Nernst potential for protons (from equation 2):

$$V_H = -\{RT/z_HF\} \cdot \ln\{[H^+]_{inside}/[H^+]_{outside}\} \approx 2.3 \cdot \log_{10}([H^+]_{inside}/[H^+]_{outside} \quad \text{(equation 8)}$$

$$V_H \approx 2.3 \cdot (pH_{inside} - pH_{outside}) \quad \text{(equation 9)}$$

Although pH electrodes are relatively easy to calibrate and mV differences are absolute, this measurement technique requires skill in both manufacturing the microelectrode and maneuvering the electrode into the cell of interest. This is moderately easy for a cell such as a barnacle muscle or squid axon,[52–55] or *Xenopus* oocyte.[28,56–60] Nevertheless, vertebrate epithelial cells[61,62] and neurons[63–70] require special instrumentation and equipment similar to perfused tubule experiments. Extracellular pH measurements also may use colorimetric indicators (Table 2), pH indicator dyes (Table 3), microelectrodes,[71,72] or vibrating microelectrodes.[73–79]

pH DYES

As indicated earlier, there are multiple compounds that can affect pH in solution. To be an effective dye that responds to pH, a compound must fundamentally be a pH buffer. However, these dye buffers have the unique properties that protonation or deprotonation of the compound results in some spectral shift. The earliest of these types of pH indicators used were those that changed visible color over a defined pH range (ie, colorimetric pH indications) (Table 3).

There also are absorbance dyes. These dyes also are pH buffers that rather than changing color, change intensity (absorbance) at defined light wavelengths.[80–82] Soon thereafter, fluorescent dyes (Table 4) such as 2',7'-bis-(2-carboxyethyl)-fluorescein (BCECF) became the intracellular pH dye of choice[83–85] owing to the ease of loading small mammalian cells and more quantitative measurements between preparations enabled by the ratio of a pH-sensitive emission to the pH-insensitive emission. This later property allows relative, and calibrated, intracellular pH to be compared across preparations regardless of dye loading efficiency. Use of the acetoxy-methyl ester of BCECF typically allows very efficient dye uptake at room temperature and 37°C. Once the acetoxy-methyl ester of BCECF is transported into cells (apparently via carboxylate or organic anion transporters), the acetoxy-methyl ester is cleaved by cellular esterases to trap BCECF in the cell. Nevertheless, no method is perfect, and with BCECF measurements it is critical to monitor both emission wavelengths to ensure that cells are healthy.[86]

GENETICALLY ENCODED pH SENSORS

With the discovery of green fluorescent protein (GFP) and other naturally fluorescent proteins (FPs), investigators have explored more of the nuanced chemistry of these FPs. Notably, GFP fluorescence intensity has an endogenous pH dependence.[87] This property was noted soon after the discovery of GFPs in the 1960s and later was exploited by Shimomura et al as a genetically encoded ion sensor recognized by the 2008 Chemistry Nobel Prize (https://www.nature.com/news/2008/081008/full/news.2008.1159.html). However, through the work of Nobel Laurette Roger Tsien, PhD (http://www.tsienlab.ucsd.edu/), and his laboratory, GFP was mutated and altered to produce the spectrum of living colors now available (http://www.clontech.com/US/Products/Fluorescent_Proteins_and_Reporters/Fluorescent_Proteins/Fluorescent_Proteins_Selection_Tool).

In 1999, Verkman and colleagues[88] reported variants of enhanced yellow fluorescent protein (eYFP) that change fluorescent intensity with halide (I^- and Cl^-) concentration. This eYFP still remained pH sensitive, but the group was able to use eYFP-stably transfected Fischer rat thyroid (FRT) epithelial cells to search for cystic fibrosis transmembrane conductance regulator inhibitors and activators.[89,90] Several modified versions of GFP, including pHluorin[91] and super ecliptic pHluorin (SEpH),[92] have been used as genetically encoded pH indicators (GEpHIs). In contrast to pH-sensitive dye, these GEpHIs may be easily modified with targeting sequences so that pH of membrane-bound cellular compartments can be measured.[93,94]

The next step in general fluorescent protein evolution was to increase brightness further. GFP and many of the other initially used fluorescent proteins tended to aggregate within cells. For tracking proteins this characteristic is moderately annoying, but for fluorescent sensor proteins (GEpHI) this tendency creates an experimental shortcoming. In particular, the aggregating GEpHIs are no longer sampling just the membrane compartment but also have their excitation and/or emission affected by the protein aggregation. The newer, fruit-named proteins (eg, mApple, mCherry, mNectarine) are engineered so that they are monomeric rather than dimeric in nature.[95–98]

Recently, GEpHI sensors have moved to mimic the ratiometric pH dyes such as BCECF. Rossano et al[99,100] developed pHerry, which is a tandem dimer of superecliptic pHlorin tethered to mCherry. Rather than being a dual excitation probe as BCECF, pHerry is a dual excitation with dual-emission sensor (Figs. 3–5; discussed later). Similar to BCECF, Zagaynova et al[101] developed a dual-excitation pH_i indicator named SypHer2. Finally, Dendra2 is a Kaede-like, monomeric, GFP-like protein which is a photoconvertible fluorescent protein (changing from green to red emission).[102] Because pHerry has been used for both in vitro and in vivo applications,[99,100,103,104] we focus on this GEpHI. pHerry initially was developed as a probe to accurately and quickly measure pH_i in *Drosophila* nerve terminals.[103,105]

Figure 3 shows that the UAS-pHerry *Drosophila* line also may be expressed selectively in renal epithelia (ie, the Malpighian tubules [MT] of *Drosophila*).[103]

Figure 3A shows the dual emission fluorescence in selected MT regions. The same NH_4^+ prepulse elaborated in Figure 1 with green and red emissions is shown in Figure 3B, followed by the fluorescent ratio in Figure 3B.

Figure 3D shows the ratio response calibrated between external pH 5.0 to 9.0, while Figure 3E shows the normalized fluorescent response over the same range. These results indicate that pHerry and the UAS-pHerry fly is generally useful as an experimental tool to quantitatively follow up pH_i in animal tissues.

To explore this further, UAS-pHerry flies were used with different MT promotors (Fig. 3A). These ex vivo experiments (dissected MTs) using a principle cell driver (*capaR-GAL4*) or a stellate cell driver (*c724-GAL4*), make it clear that the same NH_4^+ prepulse (Fig. 1B) results in cell-type–specific pH_i changes. The acid recovery phase (illustrated in Fig. 1B–d and B–d') then may be used to quantify the acid-extrusion rate (Fig. 4C) and rate per tubule area (Fig. 4D). This quantification makes it clear that even adjacent cells in an isolated epithelial tube may have quite different transport and especially acid-base transport properties.

Figure 5 illustrates that the utility of these GEpHI (ie, pHerry) are not limited to in vitro/ex vivo experiments. Under the proper conditions, pHerry may be used for in vivo pH_i imaging (Fig. 5D and H).

Even though ratiometric dyes and sensors inherently increase the fluorescent signal-to-noise ratio, they are not without experimental shortcomings. For example, in many cell and tissue types, intracellular $[Ca^{2+}]$ ($[Ca^{2+}]_i$) as well as pH_i, are both intracellular signals triggering cellular responses. In several cases, it would be ideal to track both $[Ca^{2+}]_i$ and pH_i; however, the optimal Ca^{2+} sensors also are based on green fluorescence emission (eg, GCaMP5 or GCaMP6). This of course means that the optimal Ca^{2+} sensors overlap with the optimal pH_i sensors. Consequently, there has been some additional effort to develop red-shifted pH_i-sensitive fluorescent dyes (eg, pHrodo Red[106]) and red-shifted GEpHI (eg, pH_ire[107,108]).

Although there have been early versions of red-shifted GEpHIs (eg, pHuji[109]), nevertheless, the fluorescent yield is only a fraction of that measured with the green-emission, super ecliptic pHluorin.[92] The RFP-based pHire has the significant advantage that the fluorescent

yield is similar to that of super ecliptic pHluorin.[107] This enhanced fluorescence works well in transfected mammalian cells.[107,108] and easily can be used in conjunction with spectrally distinct genetically encoded sensors or dyes. Figure 6 illustrates one such experiment with mammalian cells transfected with pH_ire (Fig. 6A) and voltage sensitive fluorescent protein (VSFP) blue (Fig. 6B, membrane potential[110–112]). The experiment in Figure 6C is the same CO_2/HCO_3^- protocol as detailed in Figure 2. TM5 cells are changed from a HEPES-buffered solution to 5% CO_2/25 mmol/L HCO_3^-(pH 7.4), which elicits acidification (red, Fig. 6C–a) and depolarization (blue, Fig. 6C–a'). To test for the presence of a Na^+ bicarbonate cotransporter,[28,61] Na^+ is replaced (0 Na^+) in the continued presence of CO_2/HCO_3^-. This change further acidifies (red, Fig. 6C–b) and hyperpolarizes the cell (blue, Fig. 6C–b'). This particular result indicates that either an electroneutral Na^+ bicarbonate cotransporter or is a Na^+/H^+ exchanger is present in the cell. Demonstrating either HCO_3^- dependence or inhibition (amiloride for Na^+/H^+ exchanger or a stilbene for a Na^+ bicarbonate cotransporter) would allow this diagnosis.

As a final note, genetically encoded sensors and dyes are tools that do not need to be used in isolation. Over the past several decades, investigators studying Ca^{2+} signaling have used Ca^{2+} dyes in combination with electrophysiology. Although this is a bit more unusual when studying pH_i, the mixing of techniques allows experimental validation as well as additional parameter evaluation while optimizing signal-to-noise ratios for the combined approaches.

PERSPECTIVES

Manipulating buffer species or making use of buffers with optical changes in response to pH_i changes allows investigators to interrogate the intracellular environment. Coupling these special buffers (dyes and GEpHI) to ion replacement experiments ± inhibitors or ± other sensors, can be used to diagnose which membrane transport proteins, channels, or pumps are involved in cellular pH_i control. Currently, the only experimental limitations are how to best couple multiple experimental tools to study multiple cells simultaneously or how to best use and develop tools for in vivo assessment.

Financial support:

National Institutes of Health grants supported the studies reviewed: T32-DK007259, T32-DK007013, F32-DK009324, R01-DK056218, R21-DK060845, R01-EY017732, R01-DK092408, and P50-DK083007/U54-DK100227.

REFERENCES

1. Mitchell P. Coupling of phosphorylation to electron and hydrogen transfer by a chemi-osmotic type of mechanism. Nature. 1961;191:144–8. [PubMed: 13771349]
2. Busa WB, Nuccitelli R. Metabolic regulation via intracellular pH. Am J Physiol. 1984;246:R409–38. [PubMed: 6326601]
3. Trivedi B, Danforth WH. Effect of pH on the kinetics of frog muscle phosphofructokinase. J Biol Chem. 1966;241:4110–2. [PubMed: 4224144]
4. Pouyssegur J, Franchi A, L'Allemain G, Paris S. Cytoplasmic pH, a key determinant of growth factor-induced DNA synthesis in quiescent fibroblasts. FEBS Lett. 1985;190:115–9. [PubMed: 4043390]

5. Pouyssegur J, Sardet C, Franchi A, L'Allemain G, Paris S. A specific mutation abolishing Na+/H+ antiport activity in hamster fibroblasts precludes growth at neutral and acidic pH. Proc Natl Acad Sci U S A. 1984;81:4833–7. [PubMed: 6087349]
6. Pouyssegur J, Chambard JC, Franchi A, Paris S, Van Obberghen-Schilling E. Growth factor activation of an amiloride-sensitive Na+/H+ exchange system in quiescent fibroblasts: coupling to ribosomal protein S6 phosphorylation. Proc Natl Acad Sci U S A. 1982;79:3935–9. [PubMed: 6287453]
7. Ganz MB, Perfetto MC, Boron WF. Effects of mitogens and other agents on rat mesangial cell proliferation, pH, and Ca2+. Am J Physiol. 1990;259:F269–78. [PubMed: 2117398]
8. Akiba T, Rocco VK, Warnock DG. Parallel adaptation of the rabbit renal cortical sodium/proton antiporter and sodium/bicarbonate cotransporter in metabolic acidosis and alkalosis. J Clin Invest. 1987;80:308–15. [PubMed: 3038953]
9. Bierman AJ, Cragoe EJ Jr, de Laat SW, Moolenaar WH. Bicarbonate determines cytoplasmic pH and suppresses mitogen-induced alkalinization in fibroblastic cells. J Biol Chem. 1988;263:15253–6. [PubMed: 2844806]
10. Boron WF. Control of intracellular pH In: Seldin DW, Giebisch G, eds. The kidney: physiology and pathophysiology, 2nd ed., New York: Raven Press; 1992:219–63.
11. Cassel D, Whiteley B, Zhuang YX, Glaser L. Mitogen-independent activation of Na+/H+ exchange in human epidermoid carcinoma A431 cells: regulation by medium osmolarity. J Cell Physiol. 1985;122:178–86. [PubMed: 3918045]
12. Eiam-Ong S, Hilden SA, Johns CA, Madias NE. Stimulation of basolateral Na(+)-HCO3- cotransporter by angiotensin II in rabbit renal cortex. Am J Physiol. 1993;265:F195–203. [PubMed: 8396341]
13. Eiam-Ong S, Hilden SA, King AJ, Johns CA, Madias NE. Endothelin-1 stimulates the Na+/H+ and Na+/HCO3- transporters in rabbit renal cortex. Kidney Int. 1992;42:18–24. [PubMed: 1321928]
14. Ganz MB, Boyarsky G, Boron WF, Sterzel RB. Effects of angiotensin II and vasopressin on intracellular pH of glomerular mesangial cells. Am J Physiol. 1988;254:F787–94. [PubMed: 3381882]
15. Ganz MB, Boyarsky G, Sterzel RB, Boron WF. Arginine vasopressin enhances pH_i regulation in the presence of HCO_3^- by stimulating three acid-base transport systems. Nature. 1989; 337:648–51. [PubMed: 2521920]
16. Ganz MB, Saksa BA. Development of pH regulatory transport in glomerular mesangial cells. Am J Physiol. 1998;274:F550–5. [PubMed: 9530271]
17. Geibel J, Giebisch G, Boron WF. Angiotensin II stimulates both Na(+)-H+ exchange and Na+/HCO3- cotransport in the rabbit proximal tubule. Proc Natl Acad Sci U S A. 1990;87: 7917–20. [PubMed: 2172967]
18. Grinstein S, Cohen S, Goetz JD, Rothstein A, Gelfand EW. Characterization of the activation of Na+/H+ exchange in lymphocytes by phorbol esters: change in cytoplasmic pH dependence of the antiport. Proc Natl Acad Sci U S A. 1985;82:1429–33. [PubMed: 2983345]
19. Humphreys BD, Jiang L, Chernova MN, Alper SL. Hypertonic activation of AE2 anion exchanger in Xenopus oocytes via NHE-mediated intracellular alkalinization. Am J Physiol. 1995; 268:C201–9. [PubMed: 7840148]
20. Moolenaar WH, Tsien RY, van der Saag PT, de Laat SW. Na+/H+ exchange and cytoplasmic pH in the action of growth factors in human fibroblasts. Nature. 1983;304:645–8. [PubMed: 6410286]
21. Preisig PA, Alpern RJ. Chronic metabolic acidosis causes an adaptation in the apical membrane Na/H antiporter and basolateral membrane Na(HCO3)3 symporter in the rat proximal convoluted tubule. J Clin Invest. 1988;82:1445–53. [PubMed: 2844858]
22. Preisig PA, Alpern RJ. Increased Na/H antiporter and Na/3HCO3 symporter activities in chronic hyperfiltration. A model of cell hypertrophy. J Gen Physiol. 1991;97:195–217. [PubMed: 1849958]
23. Romero MF. Angiotensin II mediated ion transport in the rabbit proximal tubule [PhD thesis]. Cleveland, OH: Genetics, Case Western Rerserve University; 1992.

24. Rothenberg P, Glaser L, Schlesinger P, Cassel D. Activation of Na+/H+ exchange by epidermal growth factor elevates intracellular pH in A431 cells. J Biol Chem. 1983;258:12644–53. [PubMed: 6195155]
25. Leem CH, Lagadic-Gossmann D, Vaughan-Jones RD. Characterization of intracellular pH regulation in the guinea-pig ventricular myocyte. J Physiol. 1999;517:159–80. [PubMed: 10226157]
26. Halestrap AP, Meredith D. The SLC16 gene family-from mono-carboxylate transporters (MCTs) to aromatic amino acid transporters and beyond. Pflugers Arch. 2004;447:619–28. [PubMed: 12739169]
27. Garciarena CD, Malik A, Swietach P, Moreno AP, Vaughan-Jones RD. Distinct moieties underlie biphasic H(+) gating of connexin43 channels, producing a pH optimum for intercellular communication. FASEB J. 2018;32:1969–81. [PubMed: 29183963]
28. Romero MF, Hediger MA, Boulpaep EL, Boron WF. Expression cloning and characterization of a renal electrogenic Na^+/HCO_3^- cotransporter. Nature. 1997;387:409–13. [PubMed: 9163427]
29. Romero MF, Fulton CM, Boron WF. The SLC4 gene family of HCO_3^- transporters. Pflugers Arch. 2004;447:495–509. [PubMed: 14722772]
30. Hediger MA, Mount DB, Rolfs A, Romero MF. The molecular basis of solute transport In: Brenner BM, ed. The kidney, 7th ed., Philadelphia, PA: Saunders; 2004:261–308.
31. Alper SL, Sharma AK. The SLC26 gene family of anion transporters and channels. Mol Aspects Med. 2013;34:494–515. [PubMed: 23506885]
32. Melvin JE, Park K, Richardson L, Schultheis PJ, Shull GE. Mouse down-regulated in adenoma (DRA) is an intestinal Cl^-/HCO_3^- exchanger and is up-regulated in colon of mice lacking the NHE3 Na+/H+ exchanger. J Biol Chem. 1999;274:22855–61. [PubMed: 10428871]
33. Jiang Z, Grichtchenko II, Boron WF, Aronson PS. Specificity of anion exchange mediated by mouse Slc26a6. J Biol Chem. 2002;277:33963–7. [PubMed: 12119287]
34. Ko SB, Shcheynikov N, Choi JY, et al. A molecular mechanism for aberrant CFTR-dependent HCO_3^- transport in cystic fibrosis. EMBO J. 2002;21:5662–72. [PubMed: 12411484]
35. Xie Q, Welch R, Mercado A, Romero MF, Mount DB. Molecular and functional characterization of the Slc26A6 anion exchanger, functional comparison to Slc26a1. Am J Physiol Renal Physiol. 2002;283:F826–38. [PubMed: 12217875]
36. Romero MF, Chang M-H, Plata C, et al. Physiology of electrogenic SLC26 paralogs.. Novartis Found Symp. 2006;273:126–47. [PubMed: 17120765]
37. Chang M-H, Plata C, Zandi-Nejad K, et al. Slc26A9 - anion exchanger, channel and Na^+ transporter. J Membr Biol. 2009; 128:125–40.
38. Ohana E, Yang D, Shcheynikov N, Muallem S. Diverse transport modes by the solute carrier 26 family of anion transporters. J Physiol. 2009;587:2179–85. [PubMed: 19015189]
39. Romero MF, Chen AP, Parker MD, Boron WF. The SLC4 family of bicarbonate (HCO_3^-) transporters. Mol Aspect Med. 2013;34:159–82.
40. Boron WF. Regulation of intracellular pH. Adv Physiol Educ. 2004;28:160–79. [PubMed: 15545345]
41. Roos A, Boron WF. Intracellular pH. Physiol Rev. 1981;61:296–434. [PubMed: 7012859]
42. De Vris H. Sur la permeabilité du protoplasma des betteraves rouges. Arch Neerl Sci Exactes Nat. 1871;6:118–26.
43. Nakhoul NL, Lee Hamm L. Characteristics of mammalian Rh glycoproteins (SLC42 transporters) and their role in acid-base transport. Mol Aspect Med. 2013;34:629–37.
44. Boron WF, De Weer P. Intracellular pH transients in squid giant axons caused by CO2, NH3, and metabolic inhibitors. J Gen Physiol. 1976;67:91–112. [PubMed: 1460]
45. Kikeri D, Sun A, Zeidel ML, Hebert SC. Cell membranes impermeable to NH3. Nature. 1989;339:478–80. [PubMed: 2725680]
46. Waisbren SJ, Geibel JP, Modlin IM, Boron WF. Unusual permeability properties of gastric gland cells. Nature. 1994;368: 332–5. [PubMed: 8127367]

47. Khademi S, O'Connell 3rd J, Remis J, Robles-Colmenares Y, Miercke LJ, Stroud RM. Mechanism of ammonia transport by Amt/MEP/Rh: structure of AmtB at 1.35 A. Science. 2004;305:1587–94. [PubMed: 15361618]
48. Musa-Aziz R, Chen LM, Pelletier MF, Boron WF. Relative CO2/NH3 selectivities of AQP1, AQP4, AQP5, AmtB, and RhAG. Proc Natl Acad Sci U S A. 2009;106:5406–11. [PubMed: 19273840]
49. Genetet S, Ripoche P, Picot J, et al. Human RhAG ammonia channel is impaired by the Phe65Ser mutation in overhydrated stomatocytic red cells. Am J Physiol Cell Physiol. 2012;302:C419–28. [PubMed: 22012326]
50. Assentoft M, Kaptan S, Schneider HP, Deitmer JW, de Groot BL, MacAulay N. Aquaporin 4 as a NH3 channel. J Biol Chem. 2016;291:19184–95. [PubMed: 27435677]
51. Singh SK, Binder HJ, Geibel JP, Boron WF. An apical permeability barrier to NH3/NH4+ in isolated, perfused colonic crypts. Proc Natl Acad Sci U S A. 1995;92:11573–7. [PubMed: 8524806]
52. Boron WF, Russell JM, Brodwick MS, Keifer DW, Roos A. Influence of cyclic AMP on intracellular pH regulation and chloride fluxes in barnacle muscle fibers. Nature. 1978;276:511–3. [PubMed: 31567]
53. Boron WF, McCormick WC, Roos A. pH regulation in barnacle muscle fibers: dependence on intracellular and extracellular pH. Am J Physiol. 1979;237:C185–93. [PubMed: 38672]
54. Russell JM, Boron WF. Intracellular pH regulation in squid giant axons. Kroc Found Ser. 1981;15:221–37. [PubMed: 6951945]
55. Boron WF. Transport of H+ and of ionic weak acids and bases. J Membr Biol. 1983;72:1–16. [PubMed: 6343604]
56. Fei YJ, Kanai Y, Nussberger S, et al. Expression cloning of a mammalian proton-coupled oligopeptide transporter. Nature. 1994;368:563–6. [PubMed: 8139693]
57. Gunshin H, Mackenzie B, Berger UV, et al. Cloning and characterization of a mammalian proton-coupled metal-ion transporter. Nature. 1997;388:482–8. [PubMed: 9242408]
58. Steel A, Nussberger S, Romero MF, Boron WF, Boyd CA, Hediger MA. Stoichiometry and pH dependence of the rabbit proton-dependent oligopeptide transporter PepT1. J Physiol (Lond). 1997;498:563–9. [PubMed: 9051570]
59. Nakhoul NL, Davis BA, Romero MF, Boron WF. Effect of expressing the water channel aquaporin-1 on the CO2 permeability of Xenopus oocytes. Am J Physiol. 1998;274:C543–8. [PubMed: 9486145]
60. Romero MF, Fong P, Berger UV, Hediger MA, Boron WF. Cloning and functional expression of rNBC, an electrogenic Na^+-HCO_3^- cotransporter from rat kidney. Am J Physiol. 1998;274:F425–32. [PubMed: 9486238]
61. Boron WF, Boulpaep EL. Intracellular pH regulation in the renal proximal tubule of the salamander. Basolateral HCO_3^- transport. J Gen Physiol. 1983;81:53–94. [PubMed: 6833997]
62. Boron WF, Sackin H. Measurement of intracellular ionic composition and activities in renal tubules. Annu Rev Physiol. 1983; 45:483–96. [PubMed: 6342522]
63. Thomas RC. Intracellular pH of snail neurones measured with a new pH-sensitive glass micro-electrode. J Physiol (Lond). 1974;238: 159–80. [PubMed: 4838803]
64. Thomas RC. Ionic mechanism of the H+ pump in a snail neurone. Nature. 1976;262:54–5. [PubMed: 934324]
65. Thomas RC. The role of bicarbonate, chloride and sodium ions in the regulation of intracellular pH in snail neurones. J Physiol (Lond). 1977;273:317–38. [PubMed: 23429]
66. Schwiening CJ, Thomas RC. Mechanism of pHi regulation by locust neurones in isolated ganglia: a microelectrode study. J Physiol (Lond). 1992;447:693–709. [PubMed: 1317439]
67. Deitmer JW, Schlue WR. The regulation of intracellular pH by identified glial cells and neurones in the central nervous system of the leech. J Physiol (Lond). 1987;388:261–83. [PubMed: 2821243]
68. Deitmer JW, Schlue WR. An inwardly directed electrogenic sodium-bicarbonate co-transport in leech glial cells. J Physiol (Lond). 1989;411:179–94. [PubMed: 2559193]

69. Chesler M, Nicholson C. Regulation of intracellular pH in vertebrate central neurons. Brain Res. 1985;325:313–6. [PubMed: 3978424]
70. Chesler M, Kraig RP. Intracellular pH of astrocytes increases rapidly with cortical stimulation. Am J Physiol. 1987;253:R666–70. [PubMed: 3116863]
71. Chesler M, Chan CY. Stimulus-induced extracellular pH transients in the in vitro turtle cerebellum. Neuroscience. 1988;27:941–8. [PubMed: 3252179]
72. Chen JC, Chesler M. Extracellular alkalinization evoked by GABA and its relationship to activity-dependent pH shifts in turtle cerebellum. J Physiol (Lond). 1991;442:431–46. [PubMed: 1798035]
73. Lucas WJ, Nuccitelli R. HCO 3 (−) and OH (−) transport across the plasmalemma of Chara: spatial resolution obtained using extracellular vibrating probe. Planta. 1980;150:120–31. [PubMed: 24306585]
74. Kline D, Robinson KR, Nuccitelli R. Ion currents and membrane domains in the cleaving Xenopus egg. J Cell Biol. 1983;97: 1753–61. [PubMed: 6643577]
75. Nuccitelli R, Wiley LM. Polarity of isolated blastomeres from mouse morulae: detection of transcellular ion currents. Dev Biol. 1985;109:452–63. [PubMed: 2581832]
76. Nuccitelli R, Kline D, Busa WB, Talevi R, Campanella C. A highly localized activation current yet widespread intracellular calcium increase in the egg of the frog, Discoglossus pictus. Dev Biol. 1988;130:120–32. [PubMed: 2460387]
77. Boudko DY, Moroz LL, Harvey WR, Linser PJ. Alkalinization by chloride/bicarbonate pathway in larval mosquito midgut. Proc Natl Acad Sci U S A. 2001;98:15354–9. [PubMed: 11742083]
78. Boudko DY, Moroz LL, Linser PJ, Trimarchi JR, Smith PJ, Harvey WR. In situ analysis of pH gradients in mosquito larvae using non-invasive, self-referencing, pH-sensitive microelectrodes. J Exp Biol. 2001;204:691–9. [PubMed: 11171351]
79. O'Donnell MJ, Rheault MR, Davies SA, et al. Hormonally controlled chloride movement across Drosophila tubules is via ion channels in stellate cells. Am J Physiol. 1998;274:R1039–49. [PubMed: 9575967]
80. Johnson RG, Scarpa A. Ion permeability of isolated chromaffin granules. J Gen Physiol. 1976;68:601–31. [PubMed: 11272]
81. Burnham C, Munzesheimer C, Rabon E, Sachs G. Ion pathways in renal brush border membranes. Biochim Biophys Acta. 1982;685:260–72. [PubMed: 7066312]
82. Chaillet JR, Boron WF. Intracellular calibration of a pH-sensitive dye in isolated, perfused salamander proximal tubules. J Gen Physiol. 1985;86:765–94. [PubMed: 4078557]
83. Goldfarb D, Nord EP. Asymmetric affinity of Na+-H+ antiporter for Na+ at the cytoplasmic versus external transport site. Am J Physiol. 1987;253:F959–68. [PubMed: 2825541]
84. Preisig PA, Ives HE, Cragoe EJ Jr, Alpern RJ, Rector Jr. FC. Role of the Na+/H+ antiporter in rat proximal tubule bicarbonate absorption. J Clin Invest. 1987;80:970–8. [PubMed: 2888788]
85. Boyarsky G, Ganz MB, Sterzel RB, Boron WF. pH regulation in single glomerular mesangial cells. II. Na+-dependent and -independent Cl(−)-HCO3- exchangers. Am J Physiol. 1988;255:C857–69. [PubMed: 3202154]
86. Bevensee MO, Schwiening CJ, Boron WF. Use of BCECF and propidium iodide to assess membrane integrity of acutely isolated CA1 neurons from rat hippocampus. J Neurosci Methods. 1995;58:61–75. [PubMed: 7475234]
87. Miesenböck G, De Angelis DA, Rothman JE. Visualizing secretion and synaptic transmission with pH-sensitive green fluorescent proteins. Nature. 1998;394:192. [PubMed: 9671304]
88. Jayaraman S, Teitler L, Skalski B, Verkman AS. Long-wavelength iodide-sensitive fluorescent indicators for measurement of functional CFTR expression in cells. Am J Physiol. 1999;277: C1008–18. [PubMed: 10564094]
89. Ma T, Thiagarajah JR, Yang H, et al. Thiazolidinone CFTR inhibitor identified by high-throughput screening blocks cholera toxin-induced intestinal fluid secretion. J Clin Invest. 2002; 110:1651–8. [PubMed: 12464670]
90. Ma T, Vetrivel L, Yang H, et al. High-affinity activators of cystic fibrosis transmembrane conductance regulator (CFTR) chloride conductance identified by high-throughput screening. J Biol Chem. 2002;277:37235–41. [PubMed: 12161441]

91. Miesenbock G, De Angelis DA, Rothman JE. Visualizing secretion and synaptic transmission with pH-sensitive green fluorescent proteins. Nature. 1998;394:192–5. [PubMed: 9671304]
92. Ashby MC, Ibaraki K, Henley JM. It's green outside: tracking cell surface proteins with pH-sensitive GFP. Trends Neurosci. 2004;27:257–61. [PubMed: 15111007]
93. Machen TE, Leigh MJ, Taylor C, Kimura T, Asano S, Moore HP. pH of TGN and recycling endosomes of H+/K+-ATPase-transfected HEK-293 cells: implications for pH regulation in the secretory pathway. Am J Physiol Cell Physiol. 2003;285:C205–14. [PubMed: 12660145]
94. Jankowski A, Kim JH, Collins RF, Daneman R, Walton P, Grinstein S. In situ measurements of the pH of mammalian peroxisomes using the fluorescent protein pHluorin. J Biol Chem. 2001;276: 48748–53. [PubMed: 11641408]
95. Campbell RE, Tour O, Palmer AE, et al. A monomeric red fluorescent protein. Proc Natl Acad Sci U S A. 2002;99:7877–82. [PubMed: 12060735]
96. Perriman R. Circular mRNA encoding for monomeric and polymeric green fluorescent protein. Methods Mol Biol. 2002;183:69–85. [PubMed: 12136774]
97. Karasawa S, Araki T, Yamamoto-Hino M, Miyawaki A. A green-emitting fluorescent protein from Galaxeidae coral and its monomeric version for use in fluorescent labeling. J Biol Chem. 2003;278:34167–71. [PubMed: 12819206]
98. Shaner NC, Campbell RE, Steinbach PA, Giepmans BN, Palmer AE, Tsien RY. Improved monomeric red, orange and yellow fluorescent proteins derived from Discosoma sp. red fluorescent protein. Nat Biotechnol. 2004;22:1567–72. [PubMed: 15558047]
99. Rossano A. Activity-induced cytosolic acid transients in Drosophila melanogaster motor nerve terminals [PhD thesis]. San Antonio, TX: Graduate School of Biomedical Sciences, University of Texas Health Science Center at San Antonio; 2013.
100. Rossano AJ, Kato A, Minard K, Romero MF, Macleod GT. Na+/H+ exchange via the Drosophila vesicular glutamate transporter (DVGLUT) mediates activity-induced acid efflux from presynaptic terminals. J Physiol. 2017;595:805–24. [PubMed: 27641622]
101. Zagaynova EV, Druzhkova IN, Mishina NM, Ignatova NI, Dudenkova VV, Shirmanova MV. Imaging of intracellular pH in tumor spheroids using genetically encoded sensor SypHer2. Adv Exp Med Biol. 2017;1035:105–19. [PubMed: 29080133]
102. Pakhomov AA, Martynov VI, Orsa AN, et al. Fluorescent protein Dendra2 as a ratiometric genetically encoded pH-sensor. Biochem Biophys Res Commun. 2017;493:1518–21. [PubMed: 28986251]
103. Rossano AJ, Romero MF. Optical quantification of intracellular pH in Drosophila melanogaster Malpighian tubule epithelia with fluorescent genetically encoded pH indicators. J Vis Exp. 2017;126:e55698.
104. Rossano AJ, Anderson JB, Romero MF. Ex vivo quantification of pHi in Drosophila Malpighian tubule principal cells reveals basolateral H^+ equivalent—coupled oxalate transport through likely Slc26a1 ortholog. FASEB J. 2017;81 857816.
105. Rossano AJ, Chouhan AK, Macleod GT. Genetically encoded pH-indicators reveal activity-dependent cytosolic acidification of Drosophila motor nerve termini in vivo. J Physiol. 2013; 591:1691–706. [PubMed: 23401611]
106. Colas C, Menezes S, Gutierrez-Martinez E, Pean CB, Dionne MS, Guermonprez P. An improved flow cytometry assay to monitor phagosome acidification. J Immunol Methods. 2014;412:1–13. [PubMed: 24952246]
107. Rossano AJ, Font PNC, Holmes HL, Romero MF. Characterization of pHi regulation by NBCe1/ SLC4A4 variants with known clinical phenotypes in human immortalized trabecular meshwork cells with a red-shifted genetically-encoded pH-indicator (pHire). FASEB J. 2017;31 702–3.
108. Rossano AJ, Holmes HH, Romero MF. Novel point mutation in NBCe1/SLC4A4 displays dominant-negative inhibition of wild-type NBCe1A activity in mammalian cells and xenopus oocytes. JASN Suppl. 2017;28:366.
109. Shen Y, Rosendale M, Campbell RE, Perrais D. pHuji, a pH-sensitive red fluorescent protein for imaging of exo- and endocytosis. J Cell Biol. 2014;207:419–32. [PubMed: 25385186]

110. Sakai R, Repunte-Canonigo V, Raj CD, Knopfel T. Design and characterization of a DNA-encoded, voltage-sensitive fluorescent protein. Eur J Neurosci. 2001;13:2314–8. [PubMed: 11454036]
111. Villalba-Galea CA, Sandtner W, Dimitrov D, Mutoh H, Knopfel T, Bezanilla F. Charge movement of a voltage-sensitive fluorescent protein. Biophys J. 2009;96:L19–21. [PubMed: 19167283]
112. Empson RM, Goulton C, Scholtz D, Gallero-Salas Y, Zeng H, Knopfel T. Validation of optical voltage reporting by the genetically encoded voltage indicator VSFP-Butterfly from cortical layer 2/3 pyramidal neurons in mouse brain slices. Physiol Rep. 2015;3.
113. Kanai Y, Clemencon B, Simonin A, et al. The SLC1 high-affinity glutamate and neutral amino acid transporter family. Mol Aspect Med. 2013;34:108–20.
114. Wright EM. Glucose transport families SLC5 and SLC50. Mol Aspect Med. 2013;34:183–96.
115. Donowitz M, Ming Tse C, Fuster D. SLC9/NHE gene family, a plasma membrane and organellar family of Na(+)/H(+) exchangers. Mol Aspect Med. 2013;34:236–51.
116. Montalbetti N, Simonin A, Kovacs G, Hediger MA. Mammalian iron transporters: families SLC11 and SLC40. Mol Aspect Med. 2013;34:270–87.
117. Arroyo JP, Kahle KT, Gamba G. The SLC12 family of electroneutral cation-coupled chloride cotransporters. Mol Aspect Med. 2013;34:288–98.
118. Bergeron MJ, Clemencon B, Hediger MA, Markovich D. SLC13 family of Na(+)-coupled di- and tri-carboxylate/sulfate transporters. Mol Aspect Med. 2013;34:299–312.
119. Smith DE, Clemencon B, Hediger MA. Proton-coupled oligopeptide transporter family SLC15: physiological, pharmacological and pathological implications. Mol Aspect Med. 2013; 34:323–36.
120. Forster IC, Hernando N, Biber J, Murer H. Phosphate transporters of the SLC20 and SLC34 families. Mol Aspect Med. 2013;34: 386–95.
121. Hagenbuch B, Stieger B. The SLCO (former SLC21) superfamily of transporters. Mol Aspect Med. 2013;34:396–412.
122. Koepsell H. The SLC22 family with transporters of organic cations, anions and zwitterions. Mol Aspect Med. 2013;34: 413–35.
123. Schioth HB, Roshanbin S, Hagglund MG, Fredriksson R. Evolutionary origin of amino acid transporter families SLC32, SLC36 and SLC38 and physiological, pathological and therapeutic aspects. Mol Aspect Med. 2013;34:571–85.
124. Zhao R, Goldman ID. Folate and thiamine transporters mediated by facilitative carriers (SLC19A1–3 and SLC46A1) and folate receptors. Mol Aspect Med. 2013;34:373–85.
125. Motohashi H, Inui K. Multidrug and toxin extrusion family SLC47: physiological, pharmacokinetic and toxicokinetic importance of MATE1 and MATE2-K. Mol Aspect Med. 2013;34: 661–8.

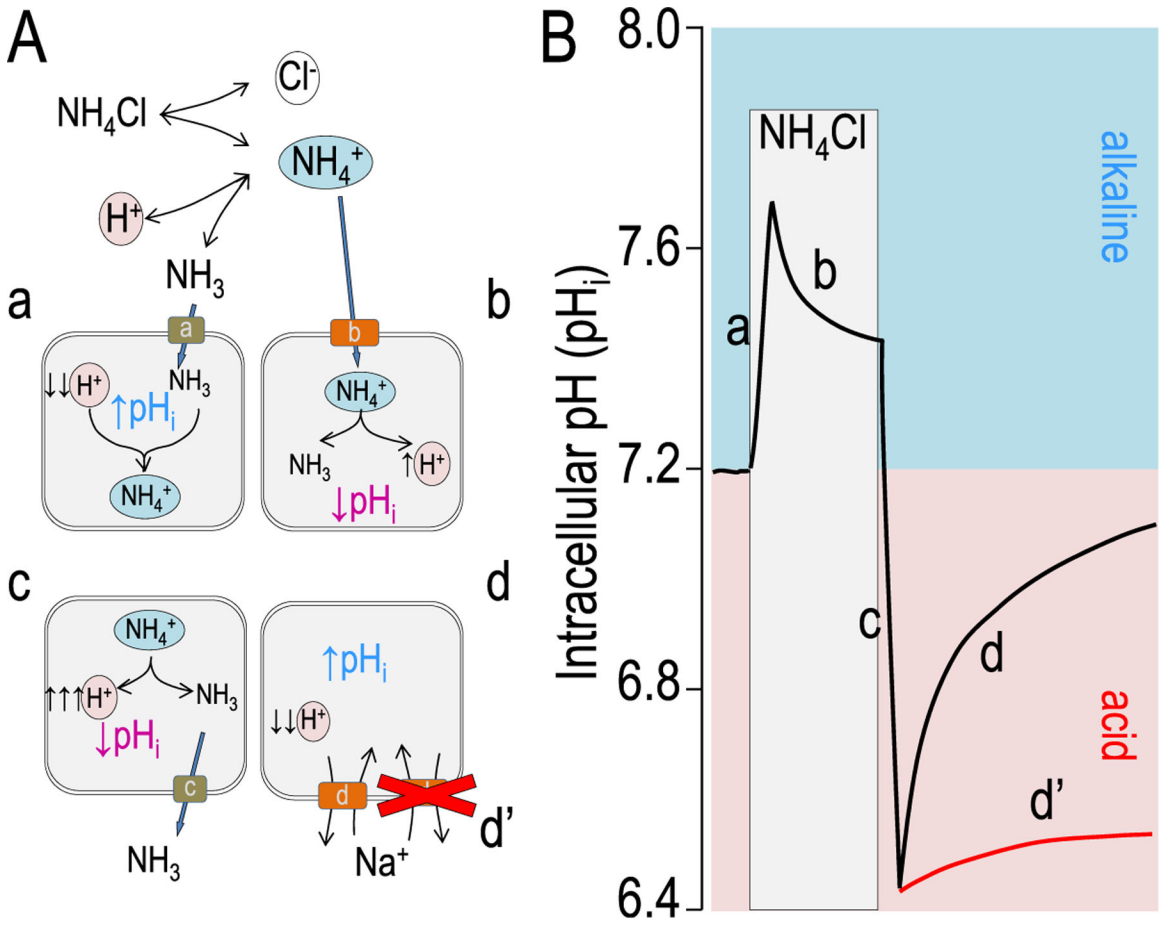

Figure 1.

Model intracellular pH (pH_i) responses to an ammonium prepulse. (A) Chemical and cellular models illustrating the buffering reaction of ammonium dissociation and reassociation [$NH_4^+ \leftrightarrow NH_3 + H^+$] as discussed in the text. Cellular models indicate the cellular chemistry and transport involved at each of the curve phases indicated in panel B. (B) A model experiment measuring pH_i is shown. The red line denotes an acid recovery in which there is either no transporter, an inactive transport, or an inhibited transporter.

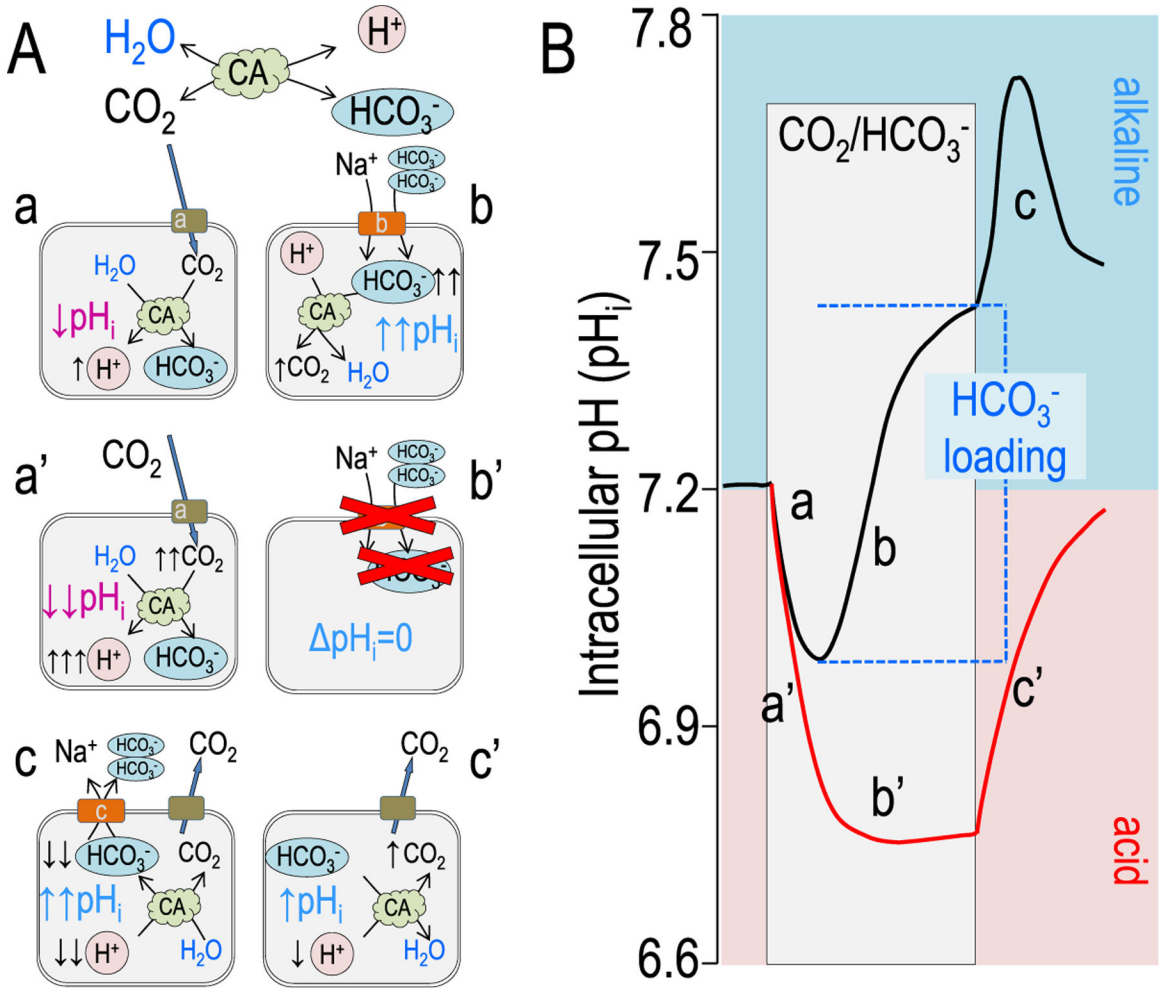

Figure 2.

Model pH_i responses form the addition of $CO_2/HCO3^-$. (A) Chemical and cellular models showing the buffering reaction of CO_2 hydration and dehydration in the presence of a carbonic anhydrase: [$CO_2 + H_2O \leftrightarrow HCO_3^- + H^+$] as discussed in the text. Cellular models indicate the cellular chemistry and transport involved at each of the curve phases indicated in panel B. (B) A model experiment measuring pH_i is shown with the acute addition of 5% CO_2/33 mmol/L HCO_3^- (pH 7.5). The red line denotes an acid recovery in which there is either no transporter, an inactive transport, or an inhibited transporter. Note that in the red trace (a'), pH_i decreases more quickly and to a more acidic pH_i because there is little cellular buffering. Similarly, without cellular HCO_3^- or H^+ transport, there is no pH_i recovery (b') (ie, alkalinization). Removal of CO_2/HCO_3^- returns pH_i to almost the initial pre-CO_2 pH_i.

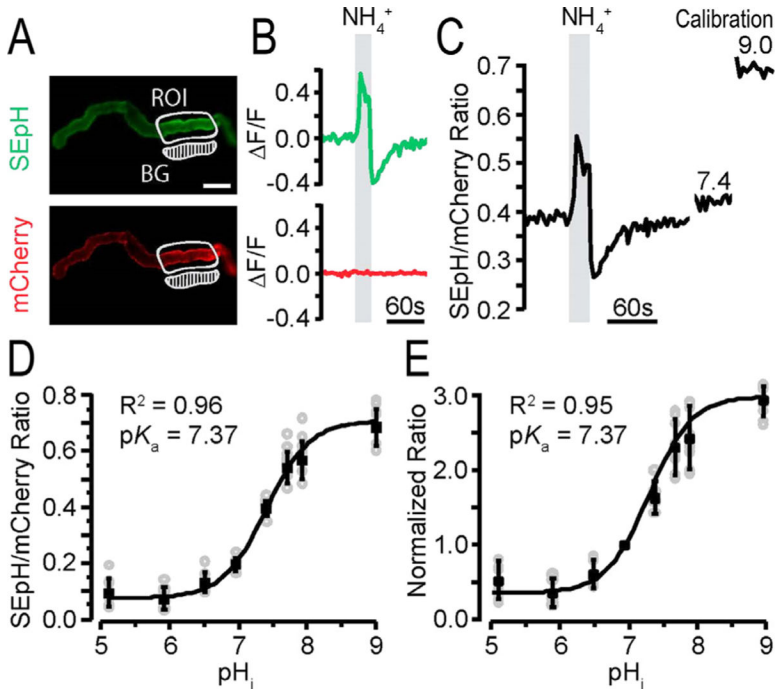

Figure 3.

Intracellular pH (pH_i) response of pHerry with NH_4Cl pulse in renal epithelia. pHerry is a genetically encoded and ratiometric pH sensor expressed in anterior Malpighian tubules (MTs) of *Drosophila*.[105] (A) Fluorescent images of pHerry (super ecliptic pHluorin [SEpH] [470/510 nm Ex/Em] and mCherry] 556/630 nm ex/em]) of UAS-pHerry driven by the *capaR-GAL4* (principle cells of MT) in healthy anterior MTs. The region of interest (ROI) is marked. The background (BG) region is indicated. Scale bar: 50 μm. (B) Relative fluorescence changes of pHerry (SEpH and mCherry signals) of pHerry after 20 seconds of 40 mmol/L NH_4Cl. The mCherry signal does not vary, it is stable, yet the SEpH signal increases fluorescence with alkalization (ie, increased pH_i) and decreases fluorescence with NH_4Cl washout (acidification; ie, decreased pH_i). (C) The ratio of fluorescent signals (SEpH/mCherry) is calculated from data in panel B after calibration (30-min incubation in calibration iPBS: 10 μmol/L nigericin, 130 mmol/L K^+, pH 7.4 and 9.0). (D) Calibration curve of the absolute pHerry ratio (SEpH/mCherry) after setting pH_i during exposure to calibration insect PBS (iPBS) at eight pH values. Gray circles are individual values from 8 preparations, and the black squares and bars are means ± SD. The curve is fit to Boltzmann distribution. (E) Same data as in panel D but normalized so that pH 7.0 has a ratio of 1.0. Reprinted with permission from Rossano and Romero.[103]

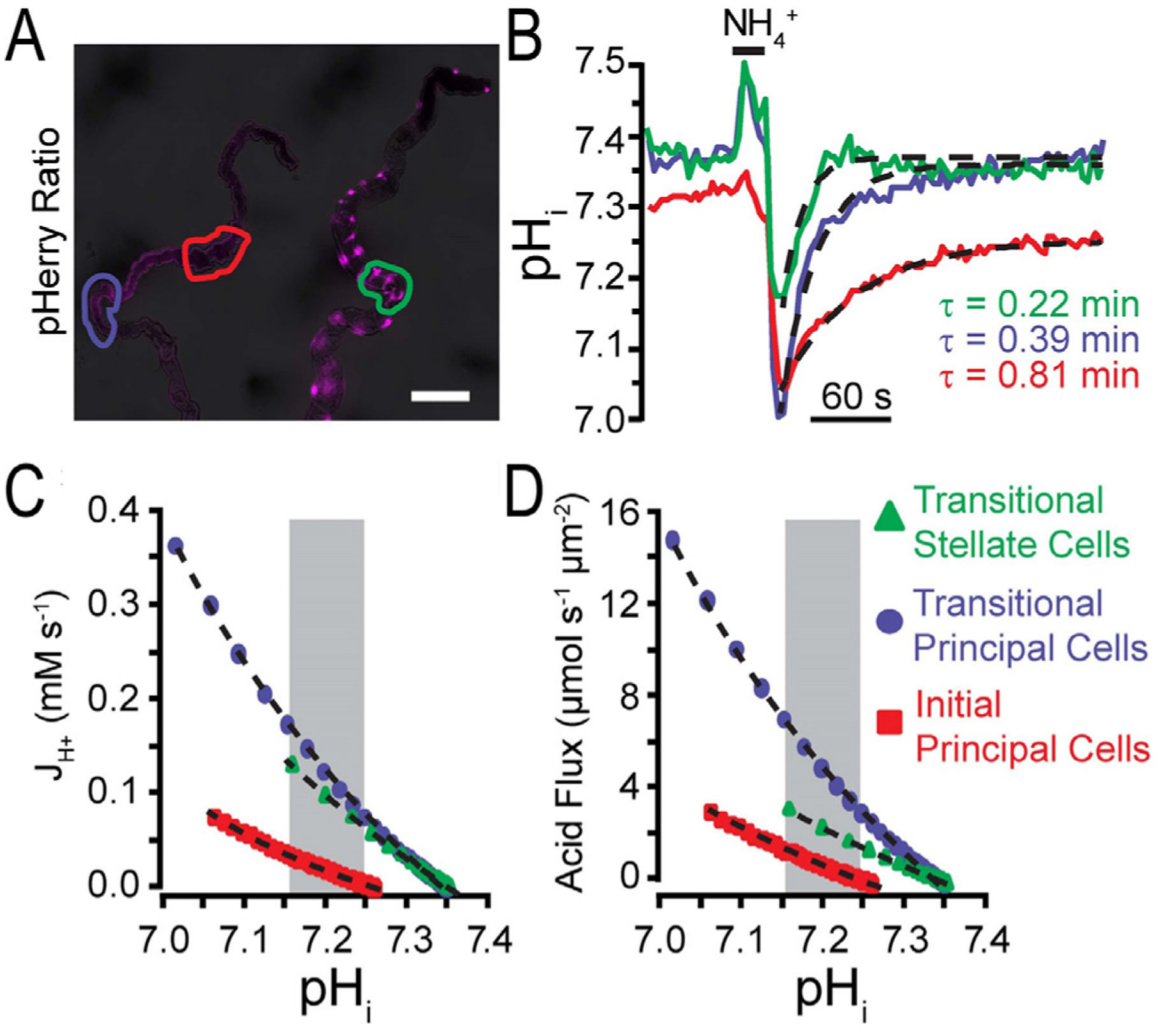

Figure 4.

Acid flux determined from pHerry responses to NH_4Cl pulse. By using pHerry, its calibration, and the rates of recovery in selected regions, a quantification of acid flux may be calculated.[103] (A) pHerry fluorescence ratio in anterior MTs: principal cells (left, driven by *capaR-GAL4*) and stellate cells (right, driven by *c724-GAL4*). Depending on MT location, stellate cells have different morphologies: cells in initial and transitional segments are bar-shaped and cells in the main segment have cellular projections. Scale bar = 100 μm. (B) pH_i changes in response to 20 seconds of 40 mmol/L NH_4Cl (in specific regions of A) are calibrated. Single exponential fits are shown as dashed curves in the acid recovery phase (withdrawal of NH_4Cl solution). The numeric fit allows a decay constant (τ) value to be derived. (C) J_{H+} (acid extrusion rate or H^+ flux) can be plotted against the calculated pH_i. (D) J_{H+} (H^+ flux) then may be transformed as a flux per unit area. Reprinted with permission from Rossano and Romero.[103]

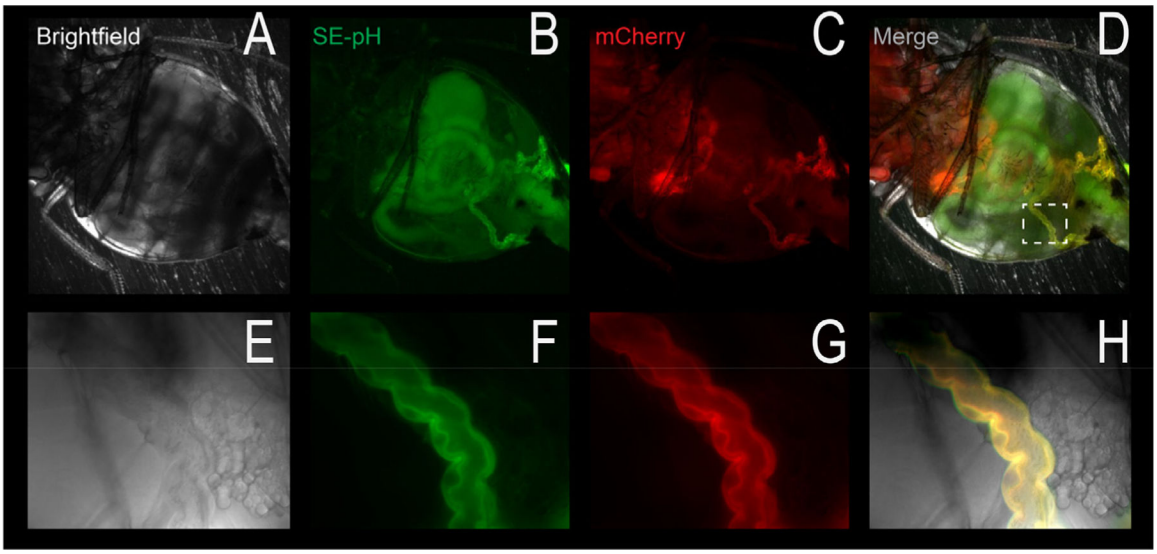

Figure 5.

In vivo pHerry fluorescence. The four panels show brightfield, super ecliptic pHluorin (SEpH) fluorescence, mCherry fluorescence, and a merge, respectively, of a living *Drosophila*. The top panels are a low magnification of the fly abdomen, which shows significant autofluorescence in the green and red channels. The dotted white box (merge panel) shows the Malpighian tubule (renal tubule epithelium, bottom images), which shows specific fluorescence, indicated by the yellow in the merged image. Note that these images were observed with the intact and anesthetized fly.

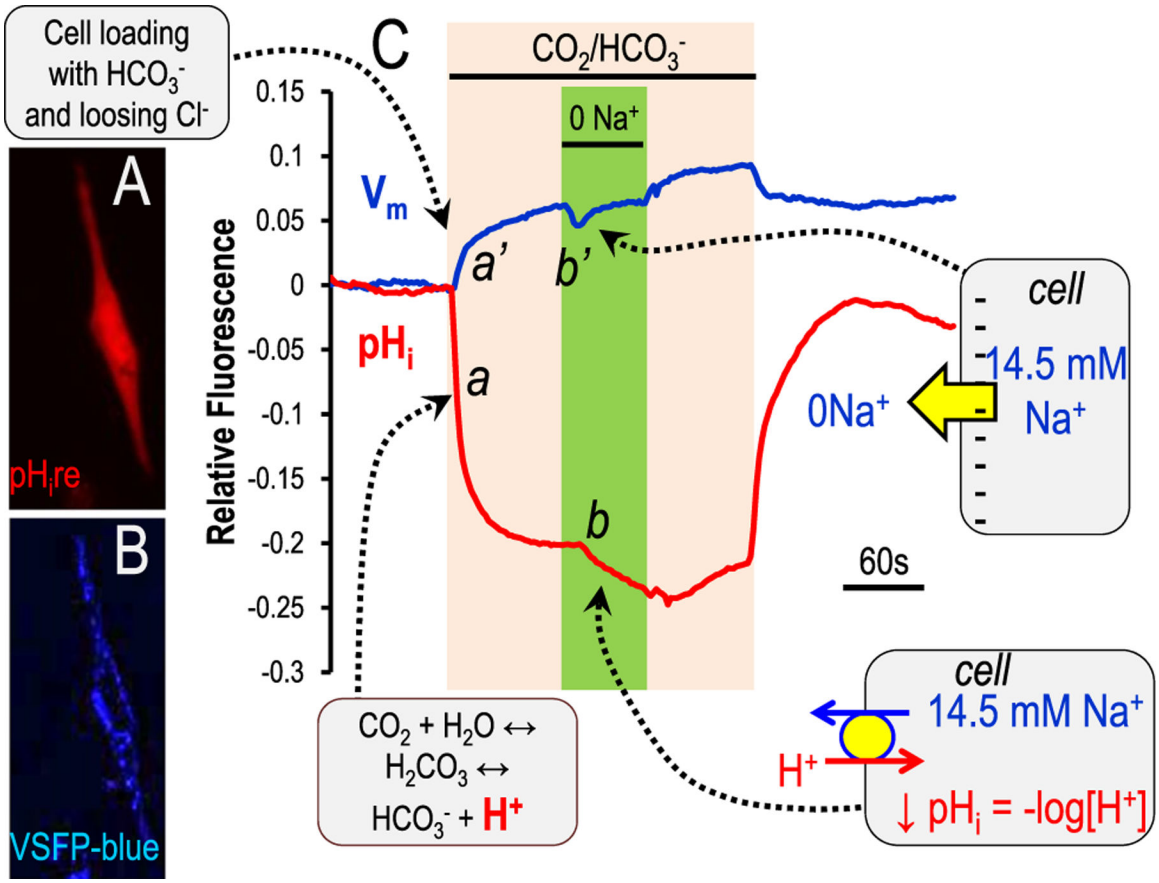

Figure 6.

Genetically encoded pH sensors in mammalian cells. The two trace lines (blue and red) illustrate relative fluorescent responses of TM5 (normal human trabecular meshwork) cells transfected with two genetically encoded sensors. Blue is VSFP blue (lower inset) and tracks membrane potential.[110–112] Red is pH_ire (upper inset) and tracks pH_i.[107] he TM5 cells on a glass coverslip were exposed to a 5% CO_2/25 mmol/L HCO_3^- (pH 7.4 at room temperature), followed by Na^+ removal (0 Na^+, replacement by choline) in the continued presence of 5% CO_2/25 mmol/L HCO_3^-. This maneuver is designed to test for the presence of a Na^+ bicarbonate cotransporter,[28,61] but also could indicate a Na^+/H^+ exchanger if HCO_3^- is not required. The callout boxes indicate the movement of ions or charge, which in turn elicit the fluorescent changes.

Table 1.

SLC Transporter Families That Move Buffer Species

SLC Family	Family Name: Transported Buffer Substrate
SLC1	Glutamate and neutral amino acids[113]: H^+, glutamate$^-$, aspartate$^-$, glutamine$^+$, asparagine$^+$
SLC4	Bicarbonate transporters[39]: HCO_3^-, CO_3^{2-} (borate)
SLC5	Na^+ glucose cotransporters[114]: SLC5 and SLC12: monocarboxylates, short-chain fatty acids, lactate$^-$, pyruvate$^-$, acetoacetate$^-$
SLC9	Na^+/H^+ exchangers[115]: H^+, NH_4^+
SLC11	H^+-coupled metal ion transporters[116]: H^+
SLC12	Electroneutral cation-coupled Cl cotransporters[117]: NH_4^+
SLC13	Na^+ sulfate/carboxylate cotransporters[118]: dicarboxylates (eg, succinate, citrate)
SLC15	H^+-coupled oligopeptide cotransporters[119]: H^+, charged peptides, β-lactam antibiotics
SLC16	Monocarboxylate transporters: H^+, monocarboxylates
SLC20/SLC34	Na^+ phosphate cotransporters[120]: $H_2PO_4^-$, HPO_4^{2-}
SLC21	Organic anion transporters[121]
SLC22	Organic cation/anion/zwitterion transporters[122]
SLC26	Multifunctional anion exchangers[31]: HCO_3^-, formate$^-$, SO_4^{2-}
SLC36	H^+-coupled amino acid transporters[123]: H^+
SLC38	System A and system N Na^+-coupled neutral amino acid transporter family[123]: H^+, charged amino acids
SLC42	Rh ammonium transporters[43]: NH_3, NH_4^+
SLC46	Folate transporters[124]: H^+
SLC47	Multidrug and toxin extrusion family[125]: tetraethylammonium

Note. Current SLC tables are available at http://slc.bioparadigms.org.

Table 2.

Biologically Important Buffering Reactions and Their pKas

Reaction	pKa
$H_2O \rightleftharpoons OH^- + H^+$	14.0
$H_2O + H_2O \rightleftharpoons OH^- + H_3O^+$	14.0
$CO_2 + H_2O \rightleftharpoons H_2CO_3 \rightleftharpoons H^+ + HCO_3^-$	6.1
$CO_2 + H_2O \rightleftharpoons H_2CO_3$	3.6
$H_2CO_3 \rightleftharpoons H^+ + HCO_3^-$	6.3
$HCO_3^- \rightleftharpoons H^+ + CO_3^{2-}$	10.32
$NH_3 + H_+ \leftrightarrow NH_4^+$	9.25
H-lactate ($CH_3CH(OH)CO_2H$) $\rightleftharpoons H^+ + CH_3CH(OH)CO_2$	3.86
H-pyruvate ($CH_3COCOOH$) $\rightleftharpoons H^+$ + pyruvate$^-$ (CH_3COCOO^-)	2.50
H-butyrate ($CH_3CH_2CH_2COOH$) $\rightleftharpoons H^+$ + butyrate$^-$ ($CH_3CH_2CH_2COOH^-$)	4.82
H-propionate (CH_3CH_2COOH) $\rightleftharpoons H^+$ + propionate$^-$ ($CH_3CH_2COOH^-$)	4.88
H-acetate (CH_3COOH) $\rightleftharpoons H^+$ + acetate$^-$ (CH_3COOH^-)	4.76
$H_3PO_4 \rightleftharpoons H_2PO_4^- + H^+$	2.14
$H_2PO_4^- \rightleftharpoons HPO_4^{2-} + H^+$	7.20
$HPO_4^{2-} \rightleftharpoons PO_4^{3-} + H^+$	12.37
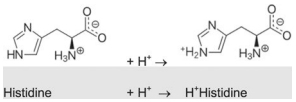	6.0–6.5

Table 3.

Colorimetric pH Indicators

Name	Acid Color	pH Range of Color Change	Base Color
Alizarin yellow R	Yellow	10.1–12.0	Red
Thymolphthalein	Colorless	9.4–10.6	Blue
Phenolphthalein	Colorless	8.2–10.0	Pink
Thymol blue	Yellow	8.0–9.6	Blue
Bromothymol blue	Yellow	6.0–7.6	Yellow
Litmus	Red	5.0–8.0	Red
Methyl red	Red	4.8–6.0	Yellow
Bromocresol green	Yellow	3.8–5.4	Blue
Methyl orange	Red	3.2–4.4	Yellow
Thymol blue (#2)	Red	1.2–2.8	Yellow
Methyl violet	Yellow	0.0–1.6	Blue

Table 4.

Indicator Dyes

pH range	pKa	Backbone Fluorophore	Ex, nm	Em, nm
6.0–8.0	7.5	SNARF	488	580 (iso) 640 (pH)
7.0–8.0	7.3	HPTS (pyranine)	410 (iso) 460 (pH)	511
6.5–7.5	6.98	BCECF	440 (iso) 490 (pH)	535
6.0–7.2	6.5	Fluorescein and carboxyfluorescein	492	514
4.5–6.0	5.2	LysoSensor green DND-189	443	505
4.2–5.7	4.7	Oregon green dyes	496	524
3.5–6.0	4.2	LysoSensor Yellow/blue DND-160	329	440
4–9 *	6.8	pHrodo Red[106]	566	590

* pHrodo succinimidyl ester shows a complex pH titration profile. Decreasing pH (from pH 9 to pH 2) produces a continuous (but nonlinear) fluorescence increase. This pH response profile typically changes upon conjugation of the dye to proteins and other biomolecules.

Abbreviations: BCECF, 2′,7′-Bis-(2-Carboxyethyl)-5-(and-6)-Carboxyfluorescein; HPTS, 8-hydroxypyrene-1,3,6-trisulfonic acid; iso, isobestic pH; pH, wavelength most sensitive to pH changes; SNARF, seminaphtorhadafluor.